Structurally driven metamagnetism in MnP and related *Pnma* compounds

Z. Gercsi and K. G. Sandeman
Department of Physics, Blackett Laboratory, Imperial College London, London SW7 2AZ, United Kingdom
(Received 26 March 2010; revised manuscript received 26 May 2010; published 21 June 2010)

We investigate the structural conditions for metamagnetism in MnP and related materials using density-functional theory. A magnetic stability plot is constructed taking into account the two shortest Mn-Mn distances. We find that a particular Mn-Mn separation plays the dominant role in determining the change from antiferromagnetic to ferromagnetic order in such systems. We establish a good correlation between our calculations and structural and magnetic data from the literature. Based on our approach it should be possible to find Mn-containing alloys that possess field-induced metamagnetism and associated magnetocaloric effects.

DOI: 10.1103/PhysRevB.81.224426 PACS number(s): 75.30.Kz, 75.80.+q, 75.30.Et, 75.30.Sg

I. INTRODUCTION

The magnetocaloric effect (MCE) is the change in temperature of a material in a changing magnetic field and was first observed in iron by Warburg.[1] It has until now been exploited in paramagnetic (PM) salts as a means of cooling below the temperature of liquid helium. However, the high global warming potential of conventional hydrofluorocarbon (HFC) refrigerants[2] and the large fraction of energy used for cooling are concerns that currently fuel interest in such magnetic cooling as a high-efficiency solid-state method of refrigeration close to room temperature. In recent years much of the search for viable room-temperature magnetic refrigerants has focused on low cost transition-metal-rich compounds that possess first-order magnetoelastic or magnetostructural phase transitions that can be driven by applied fields of the order of 1 T. Most of these materials are Mn-containing ferromagnets such as Ni_2MnGa,[3] $R_{1-x}Mn_xMnO_3$,[4] MnAs,[5] and MnFe(As,P).[6] The observation of MCEs during order-order transitions (in metamagnets) is more rare and the main examples of large effects near room temperature are in FeRh,[7] CoMnSi,[8]and Ni_2MnSn.[9] In some ways metamagnets offer a natural route to the desirably elevated MCEs associated with a first order rather than continuous magnetic transition. However, there are few metamagnets examined for their MCE that have not already been synthesized for other reasons. In this paper, we focus on MnP-type (*Pnma* space group) binary and ternary orthorhombic materials and, in particular, on what structural factors support antiferromagnetic (AFM) order and field-induced metamagnetism. Our motivation is to allow prediction of materials that may have large MCEs.

The appearance of rich magnetic features with peculiar noncollinear (NC) magnetism such as fan, helical, or cycloidal spin structures observed in MnP-type binary and the related XMnZ (TiNiSi-type) ternary alloys has engaged the interest of both theoreticians and experimentalists for several decades.[10–12] In what we term the "prototype" MnP binary alloy, the appearance of the so-called "double-helix" spiral state has been the subject of several studies. This is a state in which two pairs of Mn atoms in each cell take on the same helical wave vector but with a fixed phase difference between the pairs. Gribanov and Zavadskii[13] ascribed the occurrence of the magnetic double helix in MnP-type phases to the existence of indirect double exchange coupling. Based on an analysis of the energy stability of helimagnetic spin arrangements, Fjellvåg *et al.*[14] discussed the possibility of a metamagnetic transition by purely carrier localization with no changes in structural parameters. The complicated crystal structure of MnP is, however, a serious obstacle to a complete analysis of magnetic exchange integrals based on Goodenough's double exchange.[15] Kallel *et al.*[11] concluded that the presence of high ratios of antisymmetric to symmetric exchange is necessary to observe helical structures. They constructed a model with exchange integrals from only the nearest and second-nearest Mn separations taken into account. Dobrzynski *et al.*[16] argued that it is necessary to consider the relation of exchange interactions with up to the seventh-nearest neighbors in order to account for the magnetic structure of MnP. In TiNiSi-type ternaries, a similar complexity emerges. Studies of $Co_xNi_{1-x}MnGe$ have similarly forecast the need to consider up to eight exchange interactions, especially when a nonzero moment is present on the Co site.[12]

Despite extensive studies of the formation of noncollinear magnetic phases in MnP-based materials, no simple, guidelike explanations have been deduced that may allow the design of materials with a field-induced metamagnetic transition near to room temperature. In this paper, we compare our theoretical calculations, which use density-functional theory (DFT), with experimental findings to depict the most important structural parameters for practical material design. Our observations of high MCE and giant magnetoelastic coupling in CoMnSi (Refs. 8 and 17) and the rich variety of materials in the literature that take on the MnP (or TiNiSi) structure[18] motivate our study of metamagnetism in the MnP class.

The paper is organized as follows: in Sec. II, the underlying *Pnma* crystal structure is introduced together with the details of our computational method. Section III describes the results of *ab initio* electronic calculations based on DFT theory. We will show that the ferromagnetic (FM) structure of the prototype MnP binary alloy would undergo a change in its magnetic state as a result of isodirectional lattice expansion. This change, however can also be realized by chemical pressure through alloying as is demonstrated in Sec. IV. Examples from the literature for both 3*d* transition-metal addition as well as *p*-block partial replacement in MnP will be discussed. In Sec. V, we extend this analysis to other Mn-based ternary (TiNiSi structure) compositions that crys-

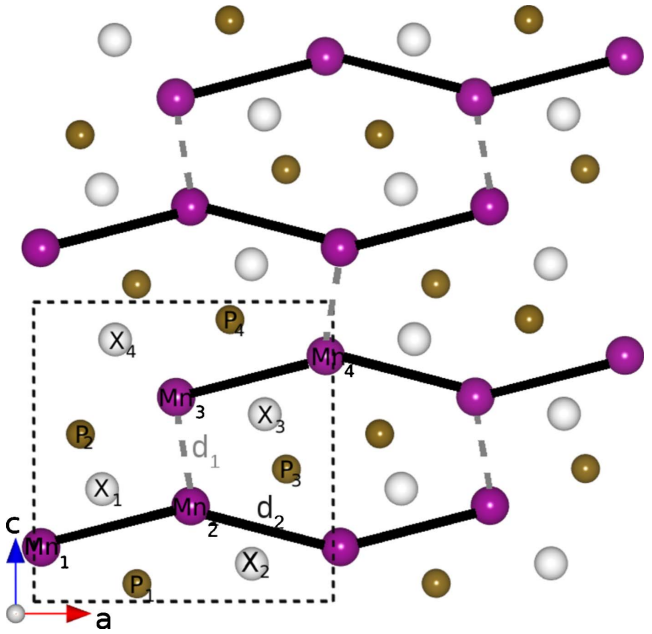

FIG. 1. (Color online) (X)MnP-type (*Pnma*, 62) orthorhombic structure [the diagram was visualized using VESTA (Ref. 19)]. The dominant d_1 and d_2 Mn-interatomic distances are constructed with dashed and solid lines, respectively.

tallize in the *Pnma* space group. Finally, we summarize the practical factors that can scale the crystal structure into the regime where a change in magnetic state can be expected.

II. CRYSTAL STRUCTURE AND COMPUTATIONAL DETAILS

A. Crystal structure

The orthorhombic crystal structure of MnP (*Pnma*, 62) is shown in Fig. 1 with unit-cell dimensions $a=5.268$ Å, $b=3.172$ Å, and $c=5.918$ Å at room temperature. Both the Mn and the P element occupy the $4c$ $(x,\frac{1}{4},z)$ crystallographic positions with $x_{\mathrm{Mn}}=0.0049(2)$, $z_{\mathrm{Mn}}=0.1965(2)$ and $x_{\mathrm{P}}=0.1878(5)$, $z_{\mathrm{P}}=0.5686(5)$.[20] The orthorhombic structure can be regarded as a distortion from the higher symmetry hexagonal NiAs ($P6_3/mmc$, 194) type structure with the atomic positions of Ni ($4c$) shifted from $x_{\mathrm{Mn}}=0$, $z_{\mathrm{Ni}}=\frac{1}{4}$ to the x_{Mn}, z_{Mn} positions and the As ($4c$) atoms moved from $x_{\mathrm{Ni}}=\frac{1}{4}$, $z_{\mathrm{Ni}}=\frac{7}{12}$ to x_{P} and z_{P}. Furthermore the two structures can be related as follows: $b_{ortho}=a_{hex}$ and $c_{ortho}=\sqrt{3}\times a_{hex}$. One direct extension of the MnP-type binary structure is the TiNiSi-type ternary with the occupation of an additional atomic species at a general $4c$ crystallographic position as shown in gray in Fig. 1. Therefore in the case of a general XMnP alloy, the number of minimal basis atoms is 4 for each species in the unit cell and assigned as Mn_{1-4} and P_{1-4} for a binary with an additional X_{1-4} element in case of a ternary alloy in Fig. 1. In addition, the two smallest Mn-Mn distances, the focus of our attention in later sections, are denoted as d_1 and d_2.

B. Computational details

The electronic-structure calculations were carried out using the VASP code based on DFT.[21] Site-based magnetic moments were calculated using the Voskown analysis within the general gradient approximation scheme. We used the minimal, eight-atom basis supercell for the binary MnP alloy with four Mn atoms and four P atoms on the $4c$ crystallographic positions, respectively, to calculate the total energies of the ferromagnetic, antiferromagnetic, and nonmagnetic (NM) states. The accurate density of states (DOS) with high density of k grid of 21, 19, and 21 points along the a, b, and c axes were used, respectively. The spin-orbit interaction was turned off during the calculations and only collinear magnetic configurations were considered. The energy convergence criterion was set to 10^{-7} eV during the energy minimization. Where applied, the expansion and compression of lattice parameters were realized isotropically.

III. RESULTS: MnP

As outlined in Sec. I, MnP exhibits complex noncollinear ferromagnetic features including low-temperature screw and conical magnetic structures, depending upon the axis of magnetization. These transform into collinear ferromagnetism at higher applied fields and temperatures.[22] The collinear ferromagnetic state is stable above $T>47$ K and it has a Curie temperature of $T_c=290$ K.[23] Such peculiar noncollinear magnetism was explained using spin-wave theory[22,23] and was more recently ascribed to the influence of magnetocrystalline anisotropy.[24] There have been several theoretical studies of both the magnetism and crystal symmetry of MnP. The first theoretical work based on augmented plane-wave theory reported ferromagnetic ground state with moments of 1.2 μ_B/f.u.,[25] in good agreement with the experimental value of 1.29 μ_B.[22] Focusing on the possibility of NiAs-MnP structural distortion, Tremel *et al.*[26] showed the importance of direct and indirect metal-metal bonding due to a second-order Jahn-Teller-type distortion within a tight-binding approach. They found that the stabilization of the lower symmetry MnP phase over the hexagonal one is due to an increased metal-metal interaction, which results in a lower density of states at the Fermi level. Spin-polarized calculations on the stability of the orthorhombic phase over the hypothetical NiAs and zinc-blende-type ones in MnP was recently also investigated[27,28] and found good agreement with experimental lattice values.

In this paper, we fix the lattice type as *Pnma* as found experimentally and concentrate on the electronic and magnetic properties of the prototype MnP binary alloy. We calculate the effect of isotropic lattice expansion and compression on NM, FM, and AFM solutions in order to find the critical lattice parameters where the crossover from one magnetic state into another can occur. For this study a single unit cell consisting of eight atoms (four Mn and four P) is used, which allows three different collinear antiferromagnetic configurations (AFM1, AFM2, and AFM3) and a collinear FM one to be constructed, as show in Table I.

Figure 2 shows the calculated total energies of the converged solutions as a function of isotropic lattice expansion and shrinkage. As is reflected from the figure, the collinear ferromagnetic state is predicted to be energetically most favorable in accordance with experimental observations (above

TABLE I. Possible collinear magnetic configurations of Mn_{1-4} in a single unit cell of MnP and their relation to d_1, d_2 inter-Mn distances.

Base atoms / Interatomic distance	Mn_1	Mn_2	Mn_3	Mn_4
	d_2		d_2	
		d_1		
FM	⇒	⇒	⇒	⇒
AFM1	⇒	⇒	⇐	⇐
AFM2	⇒	⇐	⇐	⇒
AFM3	⇒	⇐	⇒	⇐

47 K) in the range $-0.06 \lesssim \varepsilon \lesssim 0.05$. Under severe compression ($\varepsilon \lesssim -0.06$), where the closest Mn-Mn atomic distance is $d_2 \lesssim 2.55$ Å, no spontaneous magnetization is stable in the broad overlapping $3d$ bands and the calculations find convergence instead in nonmagnetic solutions. On the other hand, with lattice expansion, antiferromagnetic ground states can become more stable than the ferromagnetic one, as indicated by the crossover of the total-energy line of AFM1 around $\varepsilon \approx 0.05$ in Fig. 2. Further lattice expansion leads to the AFM3 configuration becoming the most stable one above $\varepsilon \gtrsim 0.11$ ($d_2 \lesssim 3.00$ Å). Notably, AFM2 is never favored.

The relative stability of the different magnetic ground states becomes more evident if the differences between the energies, E_{Tot} of AFM and FM states are compared ($\Delta E_{Tot} = E_{\mathrm{AFM}} - E_{\mathrm{FM}}$). By this comparison, a non-FM state becomes most favorable when it has the most negative value of ΔE_{Tot}. In Fig. 3, the regions of stability of the different magnetic states are shown as a function of Mn-Mn distance. The FM state is most stable for intermediate deformations while the nonmagnetic mode and AFM modes become favored at high compression and at high strain, respectively. Considerable magnetic moment was found only on the Mn site (M_{Mn}) as a result of exchange splitting of the d orbitals with relatively insignificant magnetic moments, $M_{\mathrm{P}} < 0.1\ \mu_B$, on the sites of P atoms. Figure 4 shows the magnetic moment of Mn atoms in the different magnetic states as a function of lattice size. In the compressed lattice region (left part of Figs. 3 and 4) the close proximity of Mn atoms causes a strong overlap of their d orbitals, resulting in broad d-d hybrid bands that cannot support spontaneous magnetization. The magnetization that grows with lattice expansion can be interpreted as a result of smaller d-d overlapping that makes the d orbitals of Mn atoms more localized. This d-orbital localization then enhances the exchange splitting of the Mn d states reflected in the increased magnetic moments.

In a compressed unit cell the p-d hybridization of P and Mn atoms can also lower the d-d exchange interaction, re-

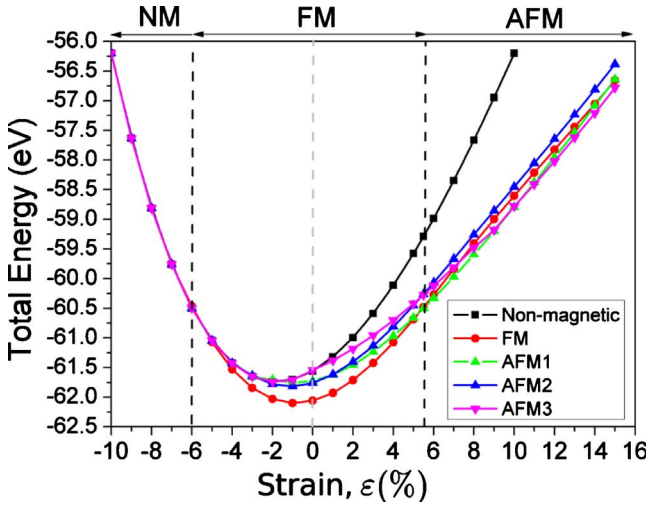

FIG. 2. (Color online) Total energy of nonmagnetic (NM), FM, and AFM solutions as a function of isotropic lattice expansion and compression in MnP.

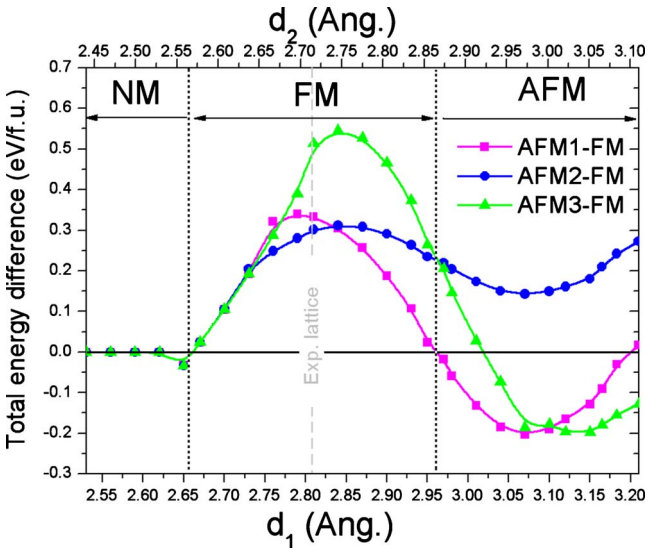

FIG. 3. (Color online) Difference between the total energies of AFM and FM solutions in MnP as a function of d_1 and d_2, the two shortest Mn-Mn separations. AFM configurations become stable where $\Delta E_{\mathrm{AFM\text{-}FM}} < 0$. The vertical dashed line represents the experimental (strain-free, $\varepsilon = 0$) Mn-separation values.

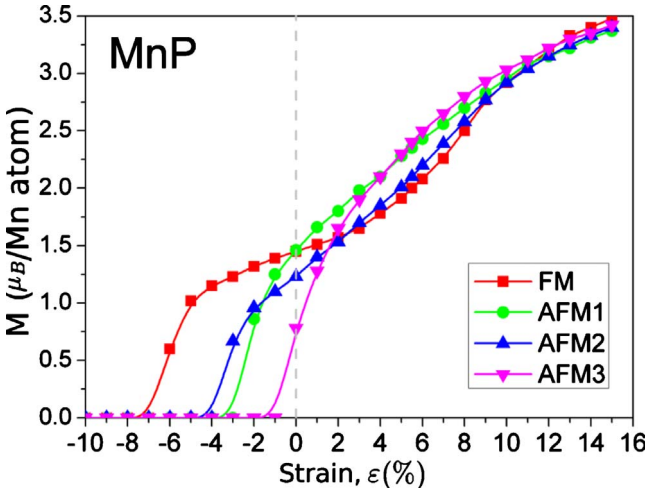

FIG. 4. (Color online) Mn magnetic moment vs strain for different magnetic states in MnP (see Table I).

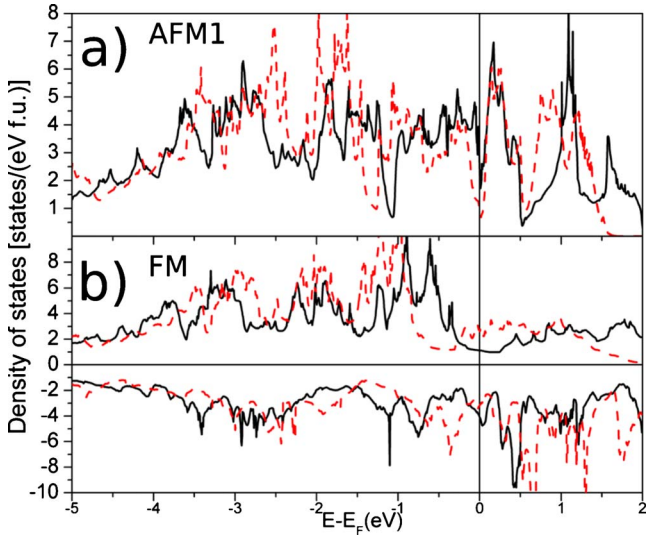

FIG. 5. (Color online) Density of states for binary MnP alloy. The total density of states at the Fermi level $[N_{Tot}(E_F)]$ decreases for antiferromagnetic (AFM1) configurations (a) with lattice expansion from $\varepsilon=0$ (solid line) to $\varepsilon=0.055$ (dashed line) while an opposite tendency is observed in (b) for FM alignment.

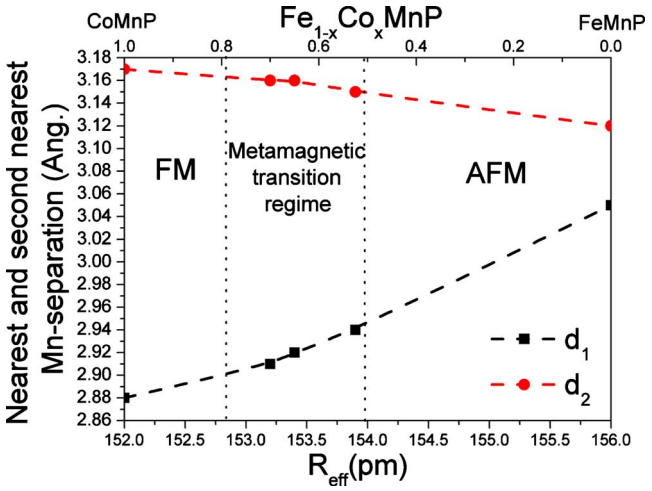

FIG. 6. (Color online) Experimentally observed Mn-Mn distances (d_1,d_2) in $(Fe_{1-x}Co_x)MnP$ pseudoternary alloy at 100 K [after (Ref. 30)]. Antiferromagnetism becomes stable as d_1 increases above ~2.95 Å, in line with our calculations on MnP in Fig. 3. Temperature-induced metamagnetism is seen for $0.5 \lesssim x \lesssim 0.8$.

ducing the magnetic moments. The enhanced exchange splitting with increased cell size is demonstrated in Fig. 5(b) (bottom), which shows the total DOS of the ferromagnetic MnP. In the equilibrium volume ($\varepsilon=0$), the main peaks of Mn d band in the majority and minority states are separated by 0.9 eV, which increases to 1.5 eV for the lattice with $\varepsilon=0.055$ lattice expansion. Simultaneously, there is an increase in the total density of states at the Fermi level, $N_{Tot}(E_F)=N_{\Downarrow}(E_F)+N_{\Uparrow}(E_F)$ in the FM state from $N_{Tot}(E_F)=5.3$ to 5.9 states/eV/f.u. However, a lowering of the DOS of the AFM1 configuration from $N_{Tot}(E_F)=5.1$ to 1.8 states/eV/f.u. can be seen, which suggests that the AFM phase is energetically more favorable Fig. 5(a) (top). In the next sections, we will show that our stability plot (Fig. 3), calculated for the binary MnP alloy can be used to predict the stability of AFM or FM states in other (X)MnZ-type binary and ternary alloys with the same (*Pnma*, 62) structure.

IV. IMPLICATIONS FOR XMnP AND Mn(P,Z)

A. (Fe,Co)MnP

A direct extension of the binary MnP alloy is the ternary FeMnP. The Fe atoms can occupy another 4*c* site without changing the orthorhombic crystal symmetry. Interestingly, the addition of iron atoms to the ferromagnetic MnP results in a commensurate noncollinear AFM structure with $T_N=340$ K. The magnetic unit cell is twice as large as the structural one, being doubled along the *c* axis with magnetic moments of $M_{Mn}=2.6\ \mu_B$ and $M_{Fe}=0.5\ \mu_B$ lying in the *ab* plane.[29] The antiferromagnetism of the system can be explained by means of the stability plot drawn for MnP in Fig. 3. The added Fe atoms cause an expansion in lattice dimensions, leading to an increase in both d_1 and d_2 inter-Mn separations into the regime where AFM coupling is stable. The resulting $d_1=3.05$ Å distance is in the proximity of the region where both AFM1 and AFM3 collinear configurations are close to the lowest point in total energy, which indicates the trend to a complex noncollinear AFM ground state.

The dominant effect of the nearest Mn-Mn distances in determining the magnetic nature of these alloys becomes more pronounced with the investigation of the pseudoternary (Co,Fe)MnP composition. $(Fe_{1-x}Co_x)MnP$ alloys exhibit complex magnetic properties ranging from noncollinear AFM for $x=0$ through temperature-induced metamagnetism for $0.5 \lesssim x \lesssim 0.8$ to collinear FM structure above $x \gtrsim 0.8$.[30] Extensive theoretical work based on Korringa-Kohn-Rostoker-coherent-potential approximation calculations by Zach *et al.*[31] tentatively explained the $N_{Tot}(E_F)$ to be partially accountable for the metamagnetic transition. Their investigation on various collinear AFM configurations found a formation of a "pseudogap" between the conduction and valence electron bands with Co addition, which results in a lowering of $N_{Tot}(E_F)$ similar to that in the strained MnP alloy of the previous section (Fig. 5).

The same authors have also tried to associate the observed magnetic states to changes in crystal structure. They found the measured Mn-(Fe,Co) and (Fe,Co)-(Fe,Co) interatomic distances to be fairly independent of temperature. The metamagnetic transition is observed in the region where $2.90 \lesssim d_1 \lesssim 2.95$ Å and $3.15 \lesssim d_2 \lesssim 3.16$ Å with a change much more visible in the d_1 distance as Fe is partially replaced by Co when compared to the change in d_2. In Fig. 6, the interatomic Mn-Mn distances (d_1,d_2) in the pseudoternary $(Fe_{1-x}Co_x)MnP$ alloy are plotted as a function of effective atomic radius. Here the effective atomic radius is defined as $R_{eff}=x\times R_{Co}+(1-x)\times R_{Fe}$, where x is the concentration, R_{Co} is the atomic radius of the Co atom (152 pm), and R_{Fe} is the atomic radius of Fe atom (156 pm), respectively. The metamagnetic transition temperature (T_t) shows a strong dependence on Co concentration. It has a value of $T_t \approx 300$ K at $x \approx 0.5$ and is completely suppressed at $x \approx 0.8$.[30] Comparison of the interatomic distances with those seen in the MnP

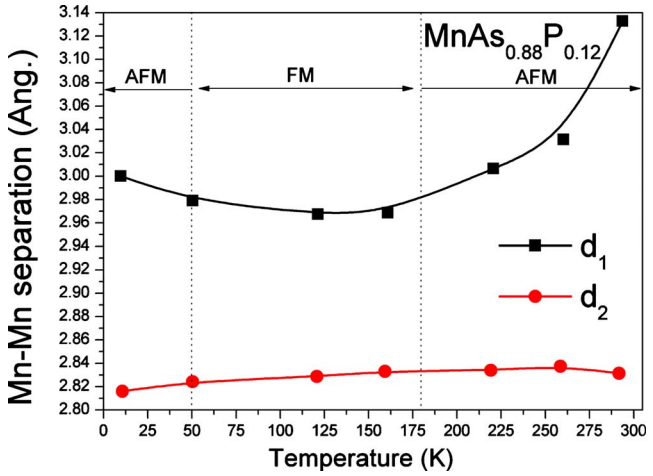

FIG. 7. (Color online) Temperature evolution of the two shortest Mn-Mn distances (d_1, d_2) in ternary $MnAs_{0.88}P_{0.12}$ pseudoternary alloy as found experimentally (Ref. 14). In accordance with Fig. 3 the AFM state is stabilized when d_1 is greater than ~2.95–2.98 Å.

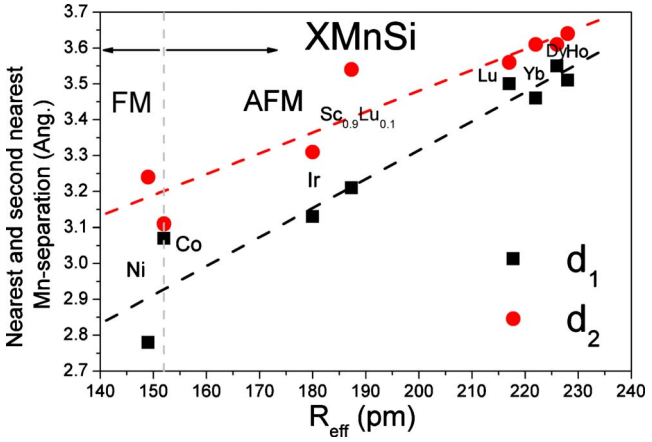

FIG. 8. (Color online) Mn-Mn separation (d_1, d_2) observed in XMnSi ternary alloys, as a function of effective X atomic radius (low-temperature data) (Refs. 17 and 36–39). Dashed lines are fitted linearly to data and are only a guide to the eye.

stability plot of Fig. 3 shows a remarkably good agreement between the theoretically expected and the experimentally found regime of AFM-FM metamagnetism. As the d_1 interatomic Mn distance is increased above ~2.95 Å the overall structure is shifted into the region where antiferromagnetism is the dominant state. This change in magnetism can also be achieved by partial replacement of the *p*-block element as demonstrated in the next section.

B. $MnAs_{1-x}P_x$

The ternary $MnAs_{1-x}P_x$ alloy is another example of metamagnetism and has been extensively studied by Fjellvåg *et al.*[14] in the $0<x<0.20$ composition range. Its rich magnetic and structural phase diagram includes the occurrence of a magnetostructural transition between hexagonal FM and PM orthorhombic phases around room temperature for $x<0.025$. That transition, in the related material in $Mn_{1-x}Fe_xAs$, recently attracted much attention due to the claims, now disputed, of an anomalously high MCE.[32] However, the interest in the origin of the crystal symmetry change is long standing. Initially, Goodenough and Kafalas[33] associated the transition of electron states of Mn atoms from high spin to low spin to the change in lattice structure from hexagonal to orthorhombic in Mn(P,As). Recently, Rungger and Sanvito[34] using detailed *ab initio* electronic-structure analysis found that if antiferromagnetic alignment in the basal plane of the hexagonal structure is imposed, the orthorhombic structure becomes more stable.

As with MnP case, we focus on magnetism within the orthogonal *Pnma* structure. Compositions around $x\approx0.10$ show complex magnetic behavior with dominant H_a-type[35] helicoidal AFM spin arrangement at low temperature that reappears at high temperatures with a transient collinear FM configuration in between. Fjellvåg and co-workers recognized the major importance of the shortest Mn-Mn separations and used neutron diffraction to map them as a function of temperature. Figure 7 reproduces the temperature dependence of d_1 and d_2 that they found in $MnAs_{0.88}P_{0.12}$. Interestingly, while the shortest Mn-Mn separation stays nearly constant at around $d_2\sim2.85$ Å, the d_1 distance shows remarkable agreement with Fig. 3: the ferromagnetic configuration shows stability over the helicoidal AFM one between $50\lesssim T\lesssim180$ K where d_1 stays below 2.95–2.98 Å. Although a direct extension of our 0 K stability criteria to finite temperatures is ambitious, the temperature-dependent magnetic behavior of $MnAs_{0.88}P_{0.12}$ suggests that the criteria we have found can be applied more generally.

The materials systems in this section exhibit a broad range of d_2 values from 2.81 Å in $MnAs_{0.88}P_{0.12}$ to 3.17 Å in $(Fe_{1-x}Co_x)MnP$. Simultaneously, d_2 changes from being the shortest to the second shortest Mn-Mn separation. Despite this change, the variety of magnetic states found in these materials seem to be well described by critical values of d_1 only, as derived from our magnetic stability plot for MnP. In the following sections, we will further extend our analysis of this plot to XMnZ-type ternary alloys with the same orthorhombic structure. The importance of the d_1 parameter in such materials will also become apparent.

V. IMPLICATIONS FOR XMnZ-TYPE ALLOYS

A. XMnSi

There is a fairly large number of XMnSi-type alloys that crystallize in the *Pnma* orthorhombic structure.[18,36–38] However, many X elements are lanthanoids of large atomic size that result in considerable expansion of the lattice. The shortest and second shortest Mn separations are plotted in Fig. 8. The high atomic radius lanthanides cause a large expansion of the *Pnma* structure and increased Mn-Mn separation, stabilizing the experimentally found AFM states in accordance with Fig. 3.

The first member of the series in which metamagnetism is observed is CoMnSi. A field-dependent metamagnetic transition from a AFM helical state to a high magnetization state was first reported in this composition by Nizioł *et al.*[40] The transition temperature can be dependent on sample prepara-

tion and was found to range from 207 to 365 K. The peculiar and complex magnetic structure has been the subject of several investigations.[12,40] Early neutron-diffraction studies found that a small magnetic moment is also developed on the Co atoms ($\sim 0.3\ \mu_B$) in addition to the major magnetic contribution from the Mn ($\sim 2.2\ \mu_B$).[40] The resulting high saturation magnetization (~ 120 emu/g at room temperature) and field-sensitive metamagnetic transition of the alloy makes it of interest as a potential room-temperature magnetic refrigerant. We previously reported a magnetic field-induced isothermal entropy change (ΔS) up to $\sim 7\ \mathrm{J\ K^{-1}\ kg^{-1}}$ around room temperature for this alloy[8] and substituted variants.[41,42] Recently, unusual negative thermal expansion along the a axis of the lattice was also observed using high-resolution neutron diffraction[17]and in the absence of an applied magnetic field a crossover in d_1 and d_2 is observed. In the above examples, and in those to follow, the critical value of d_1 parameter seems to predict well the change from FM to AFM order (around 2.95 Å). This value, however, is probably slightly increased in the case of CoMnSi, and might be associated with the additional exchange competition among the Co-Co and Co-Mn pairs, compared to the binary MnP-type alloys. As stated above, Nizioł *et al.*[12] identified up to eight important magnetic interactions responsible for the overall magnetic properties.

The end member of the XMnSi series from Fig. 8 is NiMnSi, a ferromagnet with $d_1=2.78$ Å and $d_2=3.24$ Å at 80 K.[37] The interpretation of the ferromagnetism of this ternary is apparent from the previous examples; a structure that accumulates the smaller Ni atom as a replacement for Co brings the lattice into the zone where FM coupling of Mn-Mn atoms is more stable. In the following section we show that metamagnetic behavior in more general XMnZ-type *Pnma* structures can also be designed by the partial replacement of the p-block elements.

B. $NiMnGe_{1-x}Si_x$

Using the only ferromagnetic example from the previous section, we now demonstrate that a stable AFM phase can be reintroduced even in the NiMnSi alloy by the increase in lattice dimensions with larger p-block elements. Just as with the pseudobinary $MnAs_{1-x}P_x$ in Sec. IV B, partial replacement of Si by Ge does not alter the overall valence electron number of the structure. The $NiMnGe_{1-x}Si_x$ system was studied thoroughly by Bazela *et al.*[37] and complex magnetic behavior was observed. Three regions with different types of magnetic ordering were identified as a function Si concentration: helicoidal AFM ($0 \lesssim x \lesssim 0.25$), AFM-FM-type (NC) metamagnetic ($0.3 \lesssim x \lesssim 0.55$), and collinear FM with $0.55 \lesssim x \leq 1$. d_1 and d_2 are plotted as a function of Si concentration (top scale) and effective atomic radius, R_{eff} (bottom scale) in Fig. 9. The lack of reported experimental error in the structural parameters derived from neutron-diffraction data[37] only allow us to plot a linear fit line over the data points as a guide to the eye. The validity of the stability plot calculated for MnP in Fig. 3, however, is once again manifest for such pseudoternary $NiMnGe_{1-x}Si_x$ compositions: a collinear FM state is stable for d_1 values below $d_1 \lesssim 2.95$ Å and

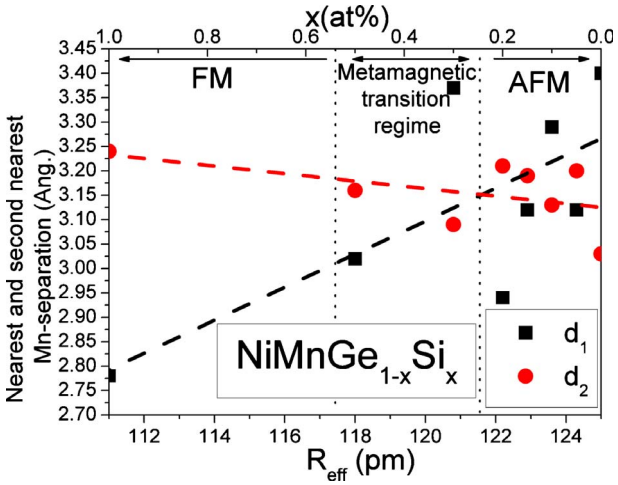

FIG. 9. (Color online) Evolution of the two shortest Mn-Mn distances (d_1, d_2) in pseudoternary $NiMnGe_{1-x}Si_x$ as a function of composition at 80 K. Field-induced metamagnetism is reported within the range $0.25 \lesssim x \lesssim 0.55$ (Ref. 37).

gives way to AFM states for $d_1 \gtrsim 2.95$ Å with increasing effective atomic size (Ge concentration).

VI. CONCLUSIONS

We have investigated the occurrence of AFM and FM states in Mn-based orthorhombic (*Pnma*, 62) alloys. Using DFT theoretical calculations based on the prototype MnP binary composition, a magnetic stability plot was constructed taking into account the two shortest Mn-Mn distances (d_1, d_2). We have correlated literature observations of different magnetic states in Mn-based *Pnma* alloys with this plot and have found a remarkable agreement. As a result of isotropic expansion the FM ground state is no longer stable but instead AFM coupling of the spins on the Mn atoms is predicted when $d_1 \gtrsim 2.95$ Å and $d_2 \gtrsim 2.88$ Å, respectively. The d_1 distance seems to play the dominant role in determining the magnetic state. In most of the samples the d_2 distance stays fairly constant as in the case of the (Co,Fe)MnP system or in the temperature dependence of the $MnAs_{0.88}P_{0.12}$ alloy. In many other cases d_2 even shows the opposite tendency to d_1, as seen in NiMn(Si,Ge). The reason for these phenomena become clearer, if one examines the *Pnma* crystal structure in Fig. 1. The Mn_1-Mn_2 atoms separated by the distance d_2 form a continuous chain along the a axis. This structural feature prefers spins on these Mn sites to be coupled antiferromagnetically by superexchange through occupied valence states along Mn-P-Mn. In fact, the magnetism along the chain probably favors AFM coupling even below the critical distance of $d_2 \approx 2.88$ Å but the theoretical calculations are based on an isotropically deformed lattice and the ratio of the a, b, and c parameters for each ε value have been fixed. Further calculations with anisotropically strained lattice needs to be carried out in order to clarify this point. The Mn atoms separated by the nearest-neighbor distance d_1 (Mn_3-Mn_4), on the other hand, do not form a continuous chain in the lattice and so short-range direct exchange is the dominant interaction. Although the competition among direct

and indirect exchanges that are also responsible for the observed noncollinearity in many of these alloys is foreseeable, the overall dominance of the direct exchange of Mn atoms along the d_1 separation was not previously evident. The key role of this separation, resulting in FM coupling for $d_1 \lesssim 2.95$ Å and AFM coupling above $d_1 \gtrsim 2.95$ Å, and its control of the overall magnetism has been shown both theoretically and by comparison of many examples from the experimental literature. Interestingly, we find this critical d_1 value, derived from binary MnP, to be influenced very little by the increased 4*c* site occupation present in *Pnma* ternaries.

Based on these findings, it should be possible to design alloys with lattice parameters tuned to a region of competition between AFM and FM states, enabling field- or temperature-driven metamagnetism. One example of such a material is Fe_xMnP with $x \approx 0.6$, where an Fe deficiency could reduce the lattice volume and bring d_1 into the proximity of FM stability. Based on our findings we believe that there is still a large number of Mn-based ternary and pseudoternary alloys that can be created with metamagnetic transitions of potential interest for their magnetocaloric effect.

ACKNOWLEDGMENTS

The research leading to these results has received funding from the European Community's Seventh Framework Programme under grant Agreement No. 214864. K.G.S. acknowledges financial support from The Royal Society. Computing resources provided by Darwin HPC and Camgrid facilities at The University of Cambridge and the HPC Service at Imperial College London are gratefully acknowledged.

[1] E. Warburg, Ann. Phys. **249**, 141 (1881).
[2] G. J. M. Velders, D. W. Fahey, J. S. Daniel, M. McFarland, and S. O. Andersen, Proc. Natl. Acad. Sci. U.S.A. **106**, 10949 (2009).
[3] L. Pareti, M. Solzi, F. Albertini, and A. Paoluzi, Eur. Phys. J. B **32**, 303 (2003).
[4] M.-H. Phan and S.-C. Yu, J. Magn. Magn. Mater. **308**, 325 (2007).
[5] H. Wada and Y. Tanabe, Appl. Phys. Lett. **79**, 3302 (2001).
[6] O. Tegus, E. Bruck, K. H. Buschow, and F. R. de Boer, Nature (London) **415**, 150 (2002).
[7] M. P. Annaorazov, K. A. Asatryan, G. Myalikgulyev, S. A. Nikitin, A. M. Tishin, and A. L. Tyurin, Cryogenics **32**, 867 (1992).
[8] K. G. Sandeman, R. Daou, S. Özcan, J. H. Durrell, N. D. Mathur, and D. J. Fray, Phys. Rev. B **74**, 224436 (2006).
[9] T. Krenke, Y. Duman, M. Acet, E. F. Wassermann, X. Moya, L. Mañosa, and A. Planes, Nature Mater. **4**, 450 (2005).
[10] T. Nagamiya, Solid State Phys. **20**, 305 (1967).
[11] A. Kallel, H. Boller, and E. F. Bertaut, J. Phys. Chem. Solids **35**, 1139 (1974).
[12] S. Nizioł, A. Bombik, W. Bażela, A. Szytuła, and D. Fruchart, J. Magn. Magn. Mater. **27**, 281 (1982).
[13] I. F. Gribanov and E. A. Zavadskii, J. Magn. Magn. Mater. **37**, 51 (1983).
[14] H. Fjellvåg, A. F. Andresen, and K. Bärner, J. Magn. Magn. Mater. **46**, 29 (1984).
[15] J. B. Goodenough, *Magnetism and the Chemical Bond* (Interscience, New York, 1963).
[16] L. Dobrzynski and A. F. Andresen, J. Magn. Magn. Mater. **82**, 67 (1989).
[17] A. Barcza, Z. Gercsi, K. Knight, and K. Sandeman, Phys. Rev. Lett. **104**, 247202 (2010).
[18] G. A. Landrum, R. Hoffmann, J. Evers, and H. Boysen, Inorg. Chem. **37**, 5754 (1998).
[19] K. Momma and F. Izumi, J. Appl. Crystallogr. **41**, 653 (2008).
[20] S. Rundqvist, Acta Chem. Scand. (1947-1973) **16**, 287 (1962).
[21] G. Kresse and J. Furthmuller, Phys. Rev. B **54**, 11169 (1996).
[22] A. Takase and T. Kasuya, J. Phys. Soc. Jpn. **47**, 491 (1979).
[23] Y. Todate, K. Yamasa, Y. Endoh, and Y. Ishukawa, J. Phys. Soc. Jpn. **56**, 36 (1987).
[24] M. S. Reis, R. M. Rubinger, N. A. Sobolev, M. A. Valente, K. Yamada, K. Sato, Y. Todate, A. Bouravleuv, P. J. von Ranke, and S. Gama, Phys. Rev. B **77**, 104439 (2008).
[25] A. Yanase and A. Hasegawa, J. Phys. C **13**, 1989 (1980).
[26] W. Tremel, R. Hoffmann, and J. Silvestre, J. Am. Chem. Soc. **108**, 5174 (1986).
[27] A. Continenza, S. Picozzi, W. T. Geng, and A. J. Freeman, Phys. Rev. B **64**, 085204 (2001).
[28] H.-M. Hong, Y.-J. Kang, J. Kang, E.-C. Lee, Y.-H. Kim, and K. J. Chang, Phys. Rev. B **72**, 144408 (2005).
[29] T. Suzuki, Y. Yamaguchi, and H. Yamamoto, J. Phys. Soc. Jpn. **34**, 911 (1973).
[30] B. Średniawa *et al.*, J. Alloys Compd. **317-318**, 266 (2001).
[31] R. Zach, J. Tobola, B. Sredniawa, S. Kaprzyk, M. Guillot, D. Fruchart, and P. Wolfers, J. Phys.: Condens. Matter **19**, 376201 (2007).
[32] A. de Campos *et al.*, Nature Mater. **5**, 802 (2006).
[33] J. B. Goodenough and J. A. Kafalas, Phys. Rev. **157**, 389 (1967).
[34] I. Rungger and S. Sanvito, Phys. Rev. B **74**, 024429 (2006).
[35] K. Selte, A. Kjekshus, and A. F. Andresen, Acta Chem. Scand. A **28a**, 61 (1974).
[36] G. Ventutini, I. ljjaali, E. Ressouche, and B. Malaman, J. Alloys Compd. **256**, 65 (1997).
[37] W. Bażela, A. Szytuła, J. Todorovic, and A. Zieba, Phys. Status Solidi A **64**, 367 (1981).
[38] T. Eriksson, L. Bergqvist, T. Burkert, S. Felton, R. Tellgren, P. Nordblad, O. Eriksson, and Y. Andersson, Phys. Rev. B **71**, 174420 (2005).
[39] I. Ijjaali, R. Welter, G. Venturini, and B. Malaman, J. Alloys Compd. **292**, 4 (1999).
[40] S. Nizioł, H. Binczycka, A. Szytuła, J. Todorovic, R. Fuchart, J. P. Senateur, and D. Fruchart, Phys. Status Solidi A **45**, 591 (1978).
[41] K. Morrison, Y. Miyoshi, J. D. Moore, A. Barcza, K. G. Sandeman, A. D. Caplin, and L. F. Cohen, Phys. Rev. B **78**, 134418 (2008).
[42] K. Morrison, J. D. Moore, K. G. Sandeman, A. D. Caplin, and L. F. Cohen, Phys. Rev. B **79**, 134408 (2009).